AGU100 ADVANCING EARTH AND SPACE SCIENCE

JGR

Journal of Geophysical Research: Atmospheres

RESEARCH ARTICLE

10.1029/2017JD028246

Key Points:

- Possible remote effects of large-scale land surface temperature in geographical areas upstream on droughts/floods have largely been ignored
- Observations show significant lagged correlation between spring surface temperature and downstream drought-flood in North America and East Asia
- North America and East Asian modeling studies show causal relationship between spring land temperature anomaly and downstream summer drought/flood

Supporting Information:

- Supporting Information S1

Correspondence to:
Y. Xue,
yxue@geog.ucla.edu

Citation:
Xue, Y., Diallo, I., Li, W., David Neelin, J., Chu, P. C., Vasic, R., et al. (2018). Spring land surface and subsurface temperature anomalies and subsequent downstream late spring-summer droughts/floods in North America and East Asia. *Journal of Geophysical Research: Atmospheres*, *123*, 5001–5019. https://doi.org/10.1029/2017JD028246

Received 28 DEC 2017
Accepted 16 APR 2018
Accepted article online 26 APR 2018
Published online 18 MAY 2018

©2018. American Geophysical Union. All Rights Reserved.

Spring Land Surface and Subsurface Temperature Anomalies and Subsequent Downstream Late Spring-Summer Droughts/Floods in North America and East Asia

Yongkang Xue[1,2], Ismaila Diallo[1], Wenkai Li[1,3,4], J. David Neelin[2], Peter C. Chu[5], Ratko Vasic[6,7], Weidong Guo[3,4], Qian Li[8], David A. Robinson[9], Yuejian Zhu[7], Congbin Fu[3,4], and Catalina M. Oaida[2]

[1]Department of Geography, University of California Los Angeles, Los Angeles, CA, USA, [2]Department of Atmospheric and Oceanic Sciences, UCLA, Los Angeles, CA, USA, [3]Institute for Climate and Global Change Research, School of Atmospheric Sciences, Nanjing University, Nanjing, China, [4]Joint International Research Laboratory of Atmospheric and Earth System Sciences, Nanjing, China, [5]Naval Ocean Analysis and Prediction Laboratory, Department of Oceanography, Naval Postgraduate School, Monterey, CA, USA, [6]I. M. Systems Group, Inc., Environmental Modeling Center/National Center for Environmental Prediction, NOAA, College Park, MD, USA, [7]Environmental Modeling Center/National Center for Environmental Prediction, NOAA, College Park, MD, USA, [8]Institute of Atmospheric Physics, Chinese Academy of Sciences, Beijing, China, [9]Department of Geography, Rutgers University, Piscataway, NJ, USA

Abstract Sea surface temperature (SST) variability has been shown to have predictive value for land precipitation, although SSTs are unable to fully predict intraseasonal to interannual hydrologic extremes. The possible remote effects of large-scale land surface temperature (LST) and subsurface temperature (SUBT) anomalies in geographical areas upstream and closer to the areas of drought/flood have largely been ignored. Here evidence from climate observations and model simulations addresses these effects. Evaluation of observational data using Maximum Covariance Analysis identifies significant correlations between springtime 2-m air temperature (T2 m) cold (warm) anomalies in both the western U.S. and the Tibetan Plateau and downstream drought (flood) events in late spring/summer. To support these observational findings, climate models are used in sensitivity studies, in which initial LST/SUBT anomaly is imposed to produce observed T2 m anomaly, to demonstrate a causal relationship for two important cases: between spring warm T2 m/LST/SUBT anomalies in western U.S. and the extraordinary 2015 flood in Southern Great Plains and adjacent regions and between spring cold T2 m/LST/SUBT anomalies in the Tibetan Plateau and the severe 2003 drought south of the Yangtze River region. The LST/SUBT downstream effects in North America are associated with a large-scale atmospheric stationary wave extending eastward from the LST/SUBT anomaly region. The effects of SST in these cases are also tested and compared with the LST/SUBT effects. These results suggest that consideration of LST/SUBT anomalies has the potential to add value to intraseasonal prediction of dry and wet conditions, especially extreme drought/flood events. The results suggest the importance of developing land data and models capable of preserving observed soil memory.

1. Introduction

Extreme climate events such as droughts and floods have substantial societal impacts and economic consequences. It is therefore important to understand the sources of such events to develop more reliable monitoring and prediction capabilities. The connection between sea surface temperature (SST) and North American droughts/floods has been extensively studied for decades. For instance, the El Niño–Southern Oscillation and the Pacific decadal oscillation phenomena in their cold (warm) phases and the Atlantic multidecadal oscillation in its warm (cold) phase produce a tendency for drought (wet) conditions over the U.S., with the Pacific Ocean playing the dominant role (e.g., Barlow et al., 2001; Schubert et al., 2009; Seager et al., 2014; Ting & Wang, 1997; Trenberthet al., 1988). Statistically significant correlations above ~0.3 at the $\alpha < 0.05$ level between Pacific SST and dry/wet in U.S. have been found (e.g., Mo et al., 2009; Rui & Wang, 2011). Despite the significant correlations, the studies consistently show that SST is only able to partially explain these phenomena (e.g., Pu et al., 2016; Scaife et al., 2009; Schubert et al., 2009; Xue, De Sales, et al., 2016). For instance, the 2016–2017 La Niña event has been associated with record rainfall that effectively ended the 5-year Californian drought, contrary to the expected SST-drought/flood relations. While atmospheric internal variability undoubtedly contributes (Hoerling et al., 2014), such exceptions underscore the

need to seek explanations beyond SST's influence alone, to pursue the identification of new mechanisms contributing to droughts/floods, which may also add value to intraseasonal prediction.

The Asian monsoon region is also greatly influenced by drought and flood events, which are associated with monsoon variability (Huang et al., 2007; Zhang & Zhou, 2015). Snow in the Himalayan mountain range and the Tibetan Plateau (TP) has been considered as one of the factors affecting the Asian monsoon variability for many decades, and snow over the Himalayas was one of the predictors in regression equations for interannual variability of the Indian monsoon (e.g., Bamzai & Shukla, 1999; Walker & Bliss, 1932). The Himalayan/TP snow-Asian monsoon relationship is also supported by a number of observational data-based analyses (e.g., Dey & Bhanu Kumar, 1983; Liu & Yanai, 2002; Wu & Qian, 2003; Xu et al., 2015; Zhao et al., 2007) and has been tested in several modeling experiments (e.g., Seol & Hong, 2009; Xiao & Duan, 2016). Although numerical experiments have demonstrated that anomalous snow cover over the Himalayas/TP had impacts on the Asian monsoon, the effects were highly variable among these studies. Moreover, the modeling sensitivity studies usually used specified extreme snow covers (such as no snow cover or double snow cover) in the experimental design or forced specified snow cover during the entire simulation time period that would violate the surface water and energy balances and affect snow impact in these studies. Robock et al. (2003) have noted that although Asian snow-albedo feedback is always operating, the anomalous snow cover impacts were not prolonged by soil moisture feedbacks. This is because the soil moisture memory is short and cannot be used as a bridge to link the winter snow cover and the subsequent summer monsoon. Furthermore, unlike the extensive and persistent Siberian snow cover, there were only a few years for which Himalayan winter snow cover anomalies persisted through the spring season (Bamzai & Shukla, 1999). Since the year 1999, Himalayan snow has no longer been used as a predictor of the Indian monsoon by the Indian Meteorological Department (Bamzai & Shukla, 1999; Thapliyal, 2001). Similar intricacies also appear in the North American snow/climate relationship (see a review in Xue et al., 2012). It seems that it could be difficult to use snow directly as a predictor for drought/flood events. However, a relationship has been shown between snow cover and surface temperature in a number of studies (e.g., Groisman et al., 2004; Karl et al., 1993; Leathers & Robinson, 1993). We conjecture that a temporally filtered response to such snow anomalies may be preserved in the land surface temperature (LST) and subsurface temperature (SUBT) anomalies. Hu and Feng (2004) used the soil temperature station data at multiple depths over the U.S. to analyze the variations of soil enthalpy, which represents integration of soil temperature through the soil column. They found that the soil enthalpy anomaly in the top 1-m soil column could persist for 2–3 months. Using the soil temperature measurements from three ground stations in TP spanning from 1981 to 2005 (Yang & Zhang, 2016) and the method presented in Entin et al. (2000) and Hu and Feng (2004), we also found that soil enthalpy anomaly in soil column of below 40 cm could persist for 3–4 months (Figure S1 in the supporting information).

We have initiated studies to explore the relationship between spring LST/SUBT anomalies and summer precipitation anomaly in North America (Xue, Oaida, et al., 2016; Xue et al., 2012). Using a general circulation model (GCM) and a regional climate model (RCM), a case study has been conducted to explore the contribution of spring LST/SUBT anomalies over the high mountain areas in western U.S. and small parts of southwest Canada (hereafter referred to as WUS) to the extraordinary 2011 summer drought of the Southern Great Plains and adjacent regions (hereafter referred to as SGP). The results suggest that the cool 2011 springtime climate conditions in the WUS increased the probability of summer drought and abnormal heat in the SGP (Xue, Oaida, et al., 2016).

The current study further explores this new mechanism and identifies spring LST/SUBT anomalies over the western high elevation areas in two continents, North America and East Asia, as a factor in creating respective late spring/summer droughts or floods in downstream regions—a concept that has been largely ignored by previous extreme hydroclimate events studies. In this paper, we first show observational evidence that identifies spatial patterns of 2-m air temperature (T2 m)-precipitation correlation that are as important as the well-known SST effects. We use T2 m for this analysis because there are no long-term large-scale LST observations that can be used to produce climatology. Second, ensemble runs with both global and regional climate models, which impose LST/SUBT anomaly as initial conditions to produce observed T2 m anomaly, are used to show causal effects of LST/SUBT for high-signal events on both continents: the 2015 SGP flood case and the 2003 East Asian drought/flood dipole pattern. The observed T2 m anomaly and the simulated T2 m anomaly are compared as constrain in these studies. These findings relating LST/SUBT anomalies to

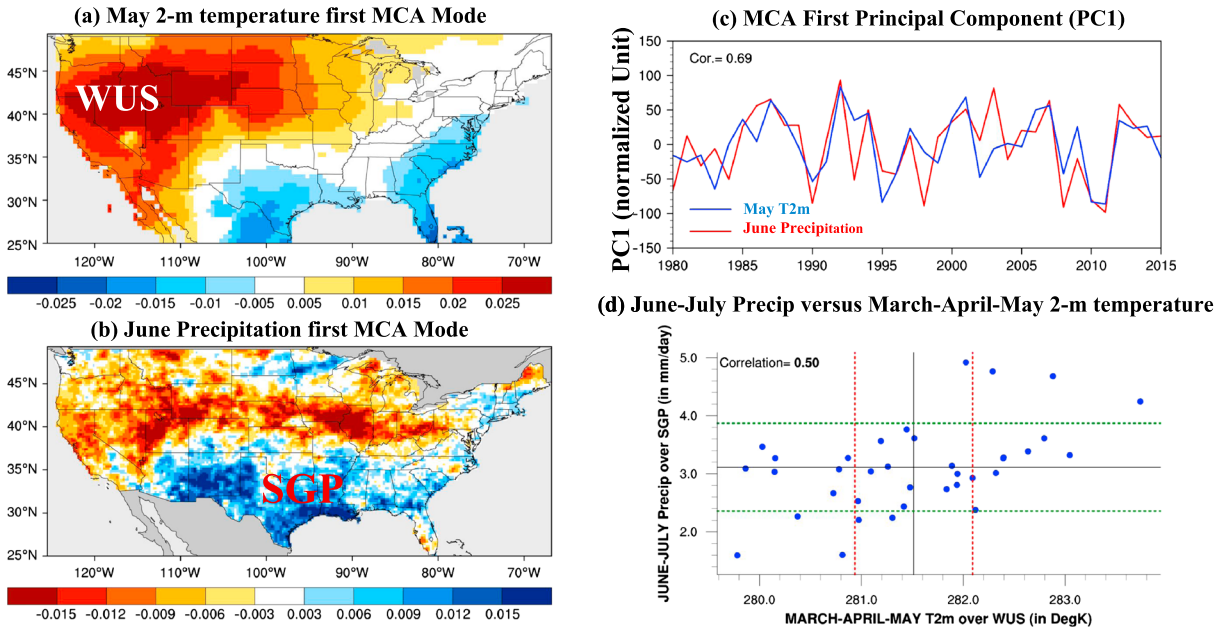

Figure 1. Maximum Covariance Analysis (MCA) over North America. (a and b) Spatial patterns of first MCA mode (MCA1) for May 2-m temperature (T2 m) and June precipitation, respectively. (c) First principal component (PC1) of MCA during 1980–2015 for May T2 m (blue line) and June precipitation (red line). (d) Scatterplots of March-April-May T2 m (in K) over western U.S. (WUS; 110–125°W/33–50°N) and June-July precipitation (in mm/day) over SGP and surrounding areas (88–103°W/29–38°N). In (d), black lines indicate means; green (red) dashed lines denote ±1 (±0.5) standard deviation boundaries for precipitation (T2 m). (a–c) are expressed in normalized unit.

downstream extreme events can serve as a new approach—complementing SST and snow anomalies—in understanding and potentially predicting such high-impact phenomena in these regions.

2. Observational Evidence

In this section, we discuss the relationship between T2 m and precipitation in North America and East Asia based on observational data, which includes the Climate Prediction Center's global gauge-based analysis of precipitation and surface temperature (GTS, Chen et al., 2002) and Climate Anomaly Monitoring System (CAMS, Ropelewski et al., 1985; Fan & Van den Dool, 2008) near-surface 2-m air temperature station data and the China Ground 2-m Temperature and Precipitation Grid Dataset (V2.0) at 0.5° × 0.5° that was produced by the National Meteorological Information Center of the China Meteorological Administration (NMIC, 2012). In the previous study, Xue, Oaida, et al. (2016) selected years with extreme warm and cold springs in WUS to identify the possible relationship between spring surface temperature anomaly and summer precipitation in the U.S. In this study, we further examine a more general relationship between these two for the period 1980–2015 in North America and East Asia using the Maximum Covariance Analysis (MCA). The MCA highlights the common spatial patterns between two variables and was previously called as the singular value decomposition analysis (Wallace et al., 1992; Von Storch & Zwiers, 1999; Xue et al., 2005). Since June is one of the months that had more drought/flood anomaly occurrences and the focus of many North American and East Asian climate studies, the MCA analysis for June precipitation and May surface temperature is presented in this paper, with its spatial and temporal patterns for North America and East Asia shown in Figures 1 and 2, respectively. The warming trend in the temperature time series was removed before the MCA analysis was performed on the data. The anomalies have been normalized by their standard deviations first, followed by MCA analyses on surface temperature/precipitation covariability.

The first North American MCA mode (MCA1) of June precipitation and May T2 m explains 36% of their squared covariance. The most distinguished May T2 m MCA1 spatial pattern (Figure 1a) is the strong anomaly over the high elevation area in WUS (Figure 1a; topography is shown for reference in Figure S2a). The most distinguished June MCA1 precipitation spatial patterns are the dipole anomalies, one over SGP and an opposite anomaly to the north (Figure 1b). The first principle component (PC1) of MCA for precipitation and T2 m

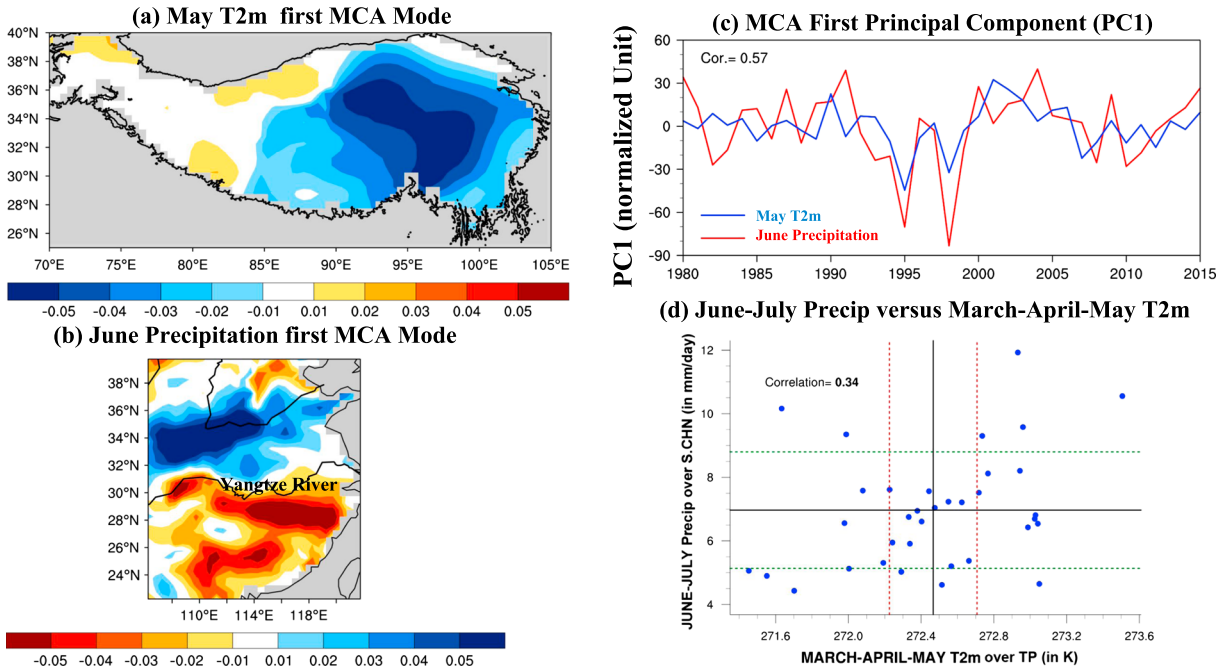

Figure 2. MCA over East Asia. (a and b) Spatial patterns of MCA1 for May T2 m over TP and June precipitation over East Asia, respectively. (c) PC1 of MCA during 1980–2015 for May T2 m (blue line) and June precipitation (red line). (d) Scatterplots of March-April-May T2 m (in K) over TP (28–37°N, 92–102°E) and June-July precipitation (in mm/day) over Yangtze River region (29–32°N, 112–121°E). In (d), black lines indicate means; green (red) dashed lines denote ±1 (±0.5) standard deviation boundaries for precipitation (T2 m). a–c are expressed in normalized unit.

PC1 (Figure 1c) is highly correlated (0.69 correlation) and exhibits pronounced interannual variations during 1980–2015. Note that the MCA and PC only show the variability; the real anomaly for each year in precipitation and T2 m is proportional to the MCA value in Figures 1a and 1b multiplied by its corresponding PC for that year in Figure 1c. When both PCs are positive (negative), both spring T2 m in WUS and summer precipitation in SGP in Figures 1a and 1b have positive (negative) anomaly, which suggests that the warm (cold) spring T2 m anomaly in WUS is associated with the summer wet (dry) conditions in SGP. This MCA analysis confirms the relationship that we found earlier (Xue, Oaida, et al., 2016) by choosing select extreme years, but with a more objective and general approach. Furthermore, we have also conducted the empirical orthogonal function (EOF) analyses (Von Storch & Zwiers, 1999; Xue et al., 2005) to identify the dominant North American spatial climate mode of May T2 m and June precipitation. It has been found that the MCA1 of June precipitation and May T2 m as shown in Figures 1a and 1b are the EOF1 of the precipitation mode (Figure S3a) and the EOF2 of the T2 m mode (Figure S3b), respectively, indicating that the MCA modes in Figures 1a and 1b are also corresponding to the main North American climate modes.

In fact, the 1 month lag relationship shown in Figure 1 is also present for other months, for instance, April T2 m in WUS versus May precipitation in SGP. However, there were few years with large May precipitation anomalies. More detailed discussions on relationships for different months are out of the scope of this paper. Instead, we show a general relationship between spring T2 m and summer precipitation in Figure 1d, which shows a scatterplot with a correlation of ~0.50 between spring (March-April-May) T2 m in WUS and summer (June-July) precipitation in SGP at $\alpha < 0.05$ significant level.

A similar analysis is also conducted for East Asia, where the high elevation TP is located in the west of the East Asian lowland plains (EALP, Figure S2b). Figures 2a and 2c show the MCA analyses for the TP May T2 m and EALP June Precipitation. The TP MCA1 (Figure 2a) shows a pronounce T2 m anomaly pattern over eastern and central TP covered by temperate steppe and shrublands. The EALP precipitation (Figure 2b) shows a dipole pattern. Based on Figure 2, negative TP T2 m MCA1 anomaly (cool) is associated with the drought over the region south of the Yangtze River and wet conditions to the north of the Yangtze River. We have also

conducted an EOF analysis to investigate the major East Asian precipitation climate mode. The precipitation MCA1 and T2 m MCA1 in this current study is similar to the precipitation EOF1 and T2 m EOF2, respectively (see Figure S4). Similar to North America, there is also a statistically significant, though weak, correlation ($\alpha < 0.05$) between TP spring (March-April-May) T2 m anomaly and summer (June-July) precipitation anomaly to the south of the Yangtze River (Figure 2d). By and large, both North America and East Asia MCA analyses performed on the historic 1980–2015 observational data suggest a general connection between a springtime T2 m anomaly over high elevation regions and a subsequent downstream summer precipitation anomaly.

3. Numerical Investigations of Causal Relationships Between Spring Surface Temperature and Summer Precipitation

The statistically significant correlations between T2 m and precipitation impelled us to further explore the causal relationship between these two variables. To achieve this goal, a modeling study is necessary. Although the MCA analyses in section 2 show a close relationship between spring T2 m in WUS and TP and late spring-summer drought/flood events downstream, the actual spatial anomaly details (locations and intensities) of T2 m and precipitation anomalies vary from year to year. To better compare with observations and explore the mechanisms, we take the case study approach. The research on T2 m/LST/SUBT effect on drought/flood is still in the incipient and exploratory stage. A similar approach of using case studies had also been taken during the early stages of SST studies (e.g., Palmer, 1986; Trenberth et al., 1988). Two case studies, including the 2011 SGP drought, had been previously investigated and described in Xue, Oaida, et al. (2016) and Xue et al. (2012) . Here we extend the T2 m/LST/SUBT effect study to East Asia and test extreme cases having different characteristics: one for the 2015 flood in North America and one for the 2003 drought/flood anomalies in East Asia.

3.1. The 2015 Flood in North America

3.1.1. Brief Background

In May 2015, precipitation anomalies in Texas and Oklahoma set a record, reaching over 200 mm above normal, about 2 times more than average. This flood event was widely reported in the media, and it had been estimated that in Houston alone the flood damage was up to about $45 million (Wang et al., 2015). From Colorado and Nebraska to Oklahoma, Texas, and Arkansas, several cities saw one of their wettest Mays on record. Based on the daily GTS data, the maximum precipitation exceeded 66 mm/week during the fourth week of May and 14 mm/day on both 24 and 26 May over the SGP area encompassing Oklahoma, Texas, Arkansas, and Louisiana. As a result, Oklahoma and Texas both had record rainfall, with 145% and 143% of the average annual precipitation, respectively, and drought conditions that began in 2010 in both states ended during 2015 (Mekonnen et al., 2016). This extreme magnitude in rainfall was not anticipated nor predicted; the cause of this extraordinary event is still largely unknown. A study has suggested that a strong El Niño event may have contributed to this record flood (Mekonnen et al., 2016).

During the winter (December–February) 2014/2015, record and near-record warmth spanned the western U.S., with six states observing record high seasonal temperatures. Much above average temperatures were also continued during the spring (Mekonnen et al., 2016). The 2014–2015 snow season saw a snow drought in the western U.S., after several years with below-normal snow (Robinson, 2015). CAMS data show that the 2015 March–April WUS T2 m was about 1.81 °C higher than the 1981–2015 mean. In particular, 2015 March T2 m was about 3.10 °C higher than average. It should be pointed out that in establishing the general lag relationship between T2 m and precipitation as presented in section 2, we only discuss the May T2 m/June precipitation and spring T2 m/summer precipitation results, because the summer, especially the month of June, was the subject of many North American and East Asian climate studies. The March–April T2 m and May Precipitation also show statistically significant correlation, and their MCA results are shown in supporting information Figure S5 for reference.

3.1.2. Experimental Design

To test the contribution of such a record-warm WUS spring T2 m to the SGP record flood event, and to compare with the SST effect, we used the WRF-NMM regional climate model (RCM, Janjic et al., 2011) with 50-km horizontal resolution and the National Center for Environmental Prediction (NCEP) Global Forecast System (GFS, Kanamitsu et al., 2002) with T126 horizontal resolution (~100 × 100 km), both of which are coupled with the Simplified Simple Biosphere model (SSiB) as the land surface model (Xue et al., 1991, 2003). The heat

transfer between subsurface and surface soil layers in SSiB is represented using a modified Force-Restore method (Deardorff, 1978; Dickinson, 1988; Xue et al., 1996). The subsurface temperature layer generally corresponds to about 1- to 2-m soil thickness depending on the vegetation types and soil conditions (Sellers et al., 1996), but its precise physical location in a soil column is hard to define. By comparing ground heat flux anomalies produced by the Force-Restore Method with a more complex model that uses a sophisticated heat transport scheme and multilayer temperature in the vertical, Mahanama et al. (2008) found that ground heat flux produced by the Force-Restore method did capture the first-order interannual variability produced by the more complex soil model. However, one of the major weaknesses of the Force-Restore Method is its deficiency in preserving the soil memory. Based on observed soil temperature data, it has been shown that the soil enthalpy anomaly in the top 1.5 m soil column in North America and TP could persist for 2–4 months (Figure S1, Hu & Feng, 2004). The simulated persistence with the Force-Restore Method, however, is only about 1 month. This shortcoming poses a challenge in the experimental design of the present study, and we will address this issue in detail in this section. We also note that there may be caveats analogous to those noted for using specified SST for interacting with surface fluxes (e.g., Barsugli & Battisti, 1998) that should be quantified if the hypothesized LST anomaly effect progresses to the stage of pragmatic prediction.

The GFS and WRF models were integrated for 2 months from 27 March to 31 May 2015 for various scenarios with seven ensemble members for each scenario. The WRF initial and lateral boundary conditions (LBC) were obtained from the corresponding NCEP-GFS cases for all scenarios, which is different from most RCM sensitivity studies, which typically use reanalysis data as LBC for both control and sensitivity runs. Our previous study (Xue et al., 2012) had demonstrated that when reanalysis data were applied as LBC in both control and anomaly runs to study the surface temperature effect, the precipitation anomalies could not be properly produced. This is because, as will be further discussed later in section 4, surface temperature affects the precipitation through perturbation of large-scale circulation. The nature of the RCM's basic design, however, is to preserve the large-scale circulation patterns that are imposed from the LBC (Xue et al., 2014). Therefore, using LBC from reanalysis for both control and sensitivity runs would suppress the surface temperature effects (Xue et al., 2012). To address this shortcoming, in the current study, the RCM LBC for a scenario was obtained from the GFS with the corresponding scenario (control and anomaly); for instance, the LBC of the RCM's control run was from the GFS's control run, which helped in capturing the large-scale circulation signature of the respective case.

Three cases were designed for this study, Case 2015_NA, Case noSUBT_NA, and Case noSST_NA, each executed using both GFS and WRF. First is the control case, from here on in referred to as Case 2015_NA, which uses the 2015 atmospheric and land initial conditions from the NCEP analyses and observed 2015 SST and sea ice for boundary conditions. Note: we will use GFS Case 2015_NA or WRF Case 2015_NA to define the run from NCEP-GFS or WRF, respectively. The similar definition to distinguish the GFS run and the WRF run will also be applied for other cases in this study. Since Reanalysis data were not available for May 2015 initial conditions by the time we started this work, the 2015 initial conditions were produced using the NCEP Global Data Assimilation System, which combines previous NCEP GFS forecast with all possible observational data. The Global Data Assimilation System is used in creating the NCEP Reanalysis and in every operational NCEP GFS initialization.

After preliminary tests, we found that the NCEP-GFS simulations failed to produce both the observed warm WUS April T2 m conditions and the May 2015 high precipitation observed across SGP. To reproduce the wet May conditions over North America, in the GFS Case 2015_NA we had to impose the specified warm LST and warm SUBT anomalies over WUS at the first time step of the model simulation (Figure 3a), after which the model updated LST and SUBT based on its free integrations. As such, the water and energy balances were preserved during the entire model integration. Because both the imposed initial LST anomaly and corresponding T2 m anomaly would disappear after a couple of days of model simulation, we had to impose initial SUBT anomalies in the model simulation, as studies have shown a high correlation between LST and SUBT (e.g., Hu & Feng, 2004). Our model simulation suggested that imposing both LST and SUBT initial anomalies was the only way that the model could produce observed T2 m anomalies, outside of specifying the observed T2 m during the entire model simulation.

Initial selections of LST/SUBT initial anomaly conditions were based on the observed T2 m difference between March 2015 (our SGP case study) and the average March value for 1981–2015. Since there is no

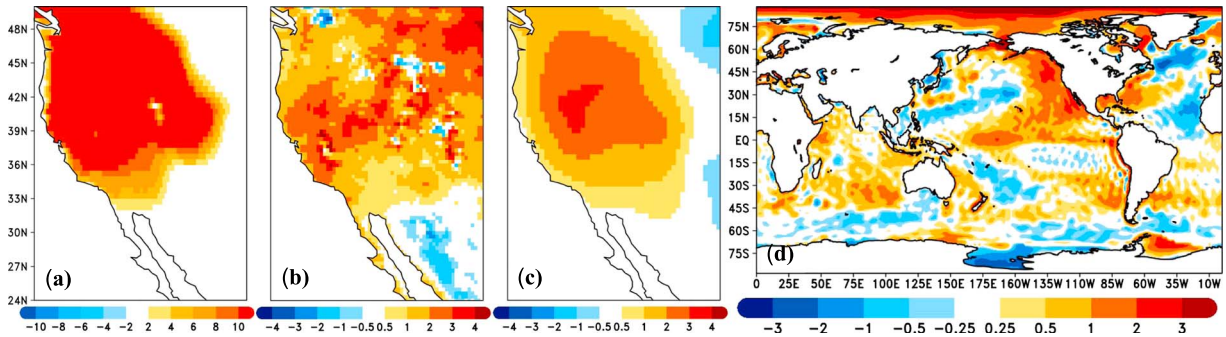

Figure 3. (a) Imposed subsurface temperature (SUBT) difference over western U.S. and Southwest Canada at the first time step of the model simulation between Case 2015_NA and Case noSUBT_NA. (b) Observed April 2 m-temperature (T2 m) anomaly between 2015 and the reference for North America. (c) NCEP-GFS-simulated April T2 m difference between Case 2015_NA and Case noSUBT_NA. (d) April 2015 SST difference between NCEP-GFS Case 2015_NA and NCEP-GFS Case noSST_NA .Unit: °C.

large-scale SUBT measurement and the Force-Restore Method fails to maintain the soil memory, which caused the imposed LST/SUBT anomaly and simulated T2 m to taper off much faster than observed T2 m anomaly, in this study we imposed SUBT anomaly based on the observed T2 m anomaly but applied the SUBT as a tuning parameter. This means that we had to decide on the magnitude of the imposed SUBT anomaly by trial and error in order to reproduce the observed monthly mean T2 m anomaly, which is the surface variable interacting with the atmosphere through directly affecting upward longwave radiation and by influencing surface heat fluxes.

The simulated May precipitation across SGP in GFS/WRF for Case 2015_NA with the above-discussed LST/SUBT initialization was about 3.61/4.66 mm/day, respectively, and was wetter than not implementing this initialization but still less than the observed value (7.47 mm/day; Figures 4a–4e). For the average over the U.S. (115–80°W and 32–49°N), the GFS produced 3.36 mm/day, while the WRF produced 3.91 mm/day,

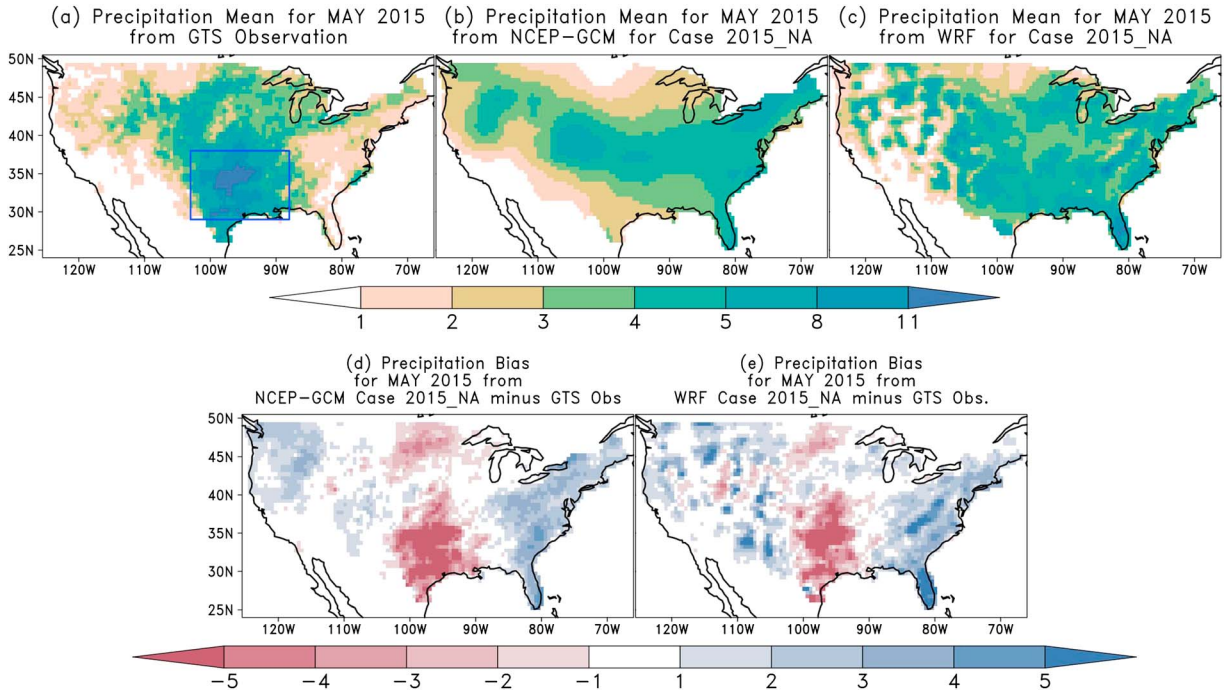

Figure 4. Mean precipitation for (a–c) May 2015 and (d and e) mean biases over United States. (a) GTS observation, (b) NCEP-GFS simulations (GFS Case 2015_NA), and (c) WRF-NMM simulations (WRF Case 2015_NA). (d) and (e) are the biases with respect to GTS observation from Case 2015_NA of NCEP-GCM and WRF-NMM, respectively. Box in (a) shows the SGP region used for precipitation regional averages. Unit: mm/day.

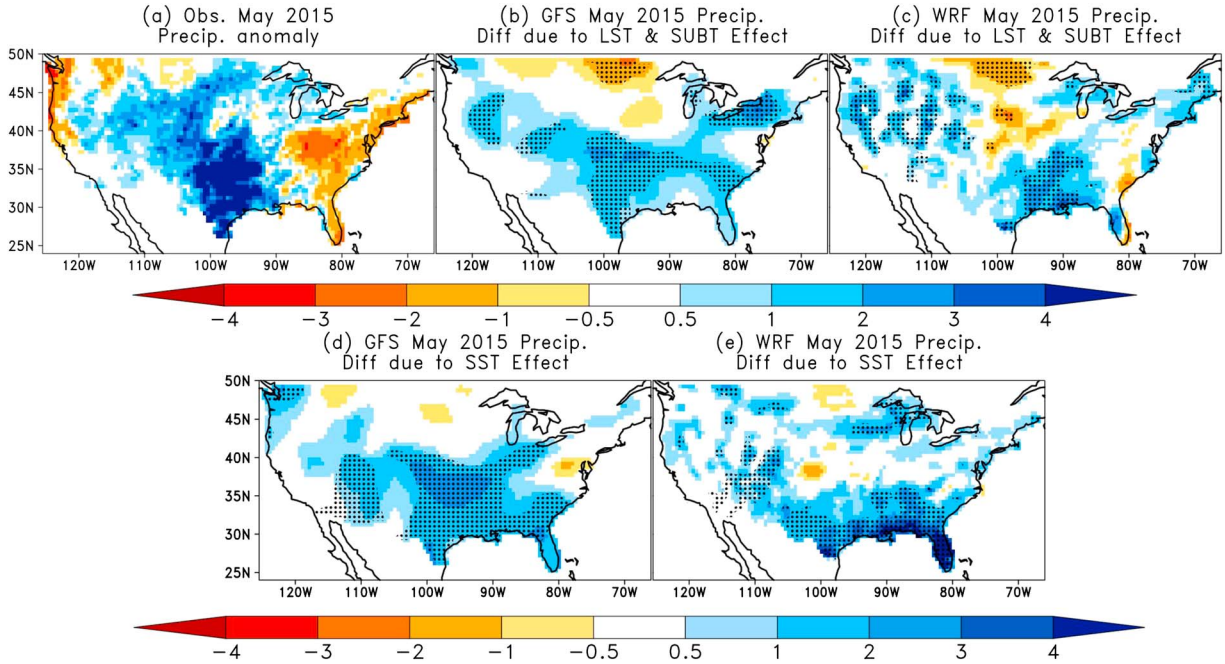

Figure 5. Observed and simulated May 2015 precipitation anomalies over the United States. (a) Observed May precipitation difference between 2015 and the reference; (b) NCEP-GCM-simulated May precipitation difference between Case 2015_NA and Case noSUBT_NA (i.e., LST and SUBT effects); (c) same as (b) but for WRF; (d) NCEP-GCM-simulated May precipitation difference between Case 2015_NA and Case noSST_NA (i.e., SST effect); (e) same as (d) but for WRF. Units: mm/day. The dotted areas denote the statistical significance at the $\alpha < 0.1$ level of *t* test values.

comparable with an observed 3.90 mm/day. WRF Case 2015_NA produced better May precipitation intensity compared to GFS Case 2015_NA (Figures 4d and 4e). Furthermore, in the GFS Case 2015_NA the heavy precipitation areas were located to the north and east compared with observations. As discussed earlier, we first tried without imposing the LST/SUBT anomaly, but it was too dry. The imposed LST/SUBT in Case 2015_NA helped produce better 2015 precipitation (Figures 3a and 4a–4e).

Furthermore, the model's dry bias would hamper the ability to investigate the SST effect. The 2015 SST has been speculated to contribute to the 2015 SGP flood (Mekonnen et al., 2016). As such, replacing the 2015 SST by, for instance, the climatology SST would be expected to lower the model-simulated SGP precipitation. However, without imposed initial LST/SUBT anomaly, the replacing of the 2015 SST by other SST would not be able to make the precipitation lower further over SGP because Case 2015_NA was already too dry there. The fact that we had to impose initial warm LST and SUBT in the control case to be able to produce the wet conditions over SGP is, in and of itself, evidence demonstrating a possible role of proper initialization of LST and SUBT in predicting intraseasonal extreme events and reveals the influence of WUS SUBT and LST anomalies on the 2015 SGP flood event in our models. More studies are needed to confirm LST/SUBT influence and identify other factors' possible role in this event.

The second case, Case noSUBT_NA, is the same as Case 2015_NA, except that the warm LST and SUBT were not imposed at the first step of the model simulations. The difference between Case 2015_NA and Case noSUBT_NA will be compared with the observed difference between the 2015 and the "reference" to assess the LST/SUBT effect on the May 2015 food event. For this purpose, the reference is selected based on the simulated T2 m difference between the control case and Case noSUBT_NA as a constraint, which could be the climatology or the mean of extreme warm/cold years (Xue, Oaida, et al., 2016; Xue et al., 2012). In this 2015 North American case, the simulated April T2 m difference between Case 2015_NA and Case noSUBT_NA was 1.82 °C over WUS. The observed surface T2 m difference there between April 2015 and climatology was 1.72 °C, while the observed T2 m difference between the April 2015 and past extreme cold years was 2.22 °C. Therefore, the climatology was a reasonable choice as a reference in this case. The observed difference between 2015 May precipitation and reference (i.e., climatology) will be compared with the precipitation difference between Case 2015_NA and Case noSUBT_NA to assess the 2015 LST/SUBT anomaly effect.

Table 1
SST and Initial SUBT Conditions for Different North American Cases

Cases	Initial SUBT conditions	SST boundary conditions	Note
Case 2015_NA	Imposing anomaly. Figure 3a	2015 SST	North American control (CTRL) case
Case noSUBT_NA	No imposed anomaly	2015 SST	North American control case minus this case shows SUBT effect.
Case noSST_NA	Same as case 2015_NA	Reference SST	North American control case minus this case shows SST effect.

The third case, Case noSST_NA, is the same as Case 2015_NA, but instead of forcing the model with the observed 2015 SST conditions, the daily SST reference was used. Here to be comparable with the LST/SUBT effect, climatological SST was imposed as the reference. The difference between Case 2015_NA and Case noSST_NA will be used to assess the 2015 SST anomaly effect. Please note that the reference selection only affects which observed anomaly will be used to assess the LST/SUBT effect and which SST will be used for the SST test. The effects of LST/SUBT as shown in the difference between Case 2015_NA and Case noSUBT_NA would not be affected. Figure 3d displays the April SST difference between GFS Case 2015_NA and GFS Case noSST_NA. The most striking SST difference in Figure 3d is the El Niño feature in the Pacific Ocean, including the warm SST along the North American coastal areas. The difference between Case 2015_NA and Case noSST_NA should provide information on how influential 2015 SST conditions were on the 2015 flood. The differences between Case 2015_NA and Case noSUBT_NA and between Case 2015_NA and Case noSST_NA can then be further compared to the observed May 2015 precipitation anomaly (Figure 5a) to assess the LST/SUBT and SST impacts, respectively. These experiments are listed in Table 1, and a detailed discussion of their results is presented in the following section.

3.1.3. LST/SUBT Effects

The observed anomaly between May 2015 and the reference shows heavy rain in Texas and Oklahoma and the areas to the northwest, while a slight dry anomaly is located to the east (Figure 5a). This east-west contrast has been found in the May precipitation MCA analysis as well (Figure S5). The differences between Case 2015_NA and Case noSUBT_NA showed that the springtime warm LST and SUBT anomalies over WUS produced statistically significant wet May conditions in Texas and Oklahoma and areas to their northwest (Figures 5b and 5c), consistent with observed anomaly (Figure 5a). The GFS under the LST/SUBT effect produced wet condition over SGP, but the eastern U.S. is too wet, about 0.96 mm/day averaged over 85–75°W and 29–38°N (Figure 5b). In contrast, the observed anomaly was about −1.10 mm/day there. WRF produced a better spatial anomaly pattern (Figure 5c) compared to the observed anomaly (Figure 5a). The precipitation difference in the eastern U.S. in Figure 5b was only 0.14 mm/day. The LST/SUBT effect produced about 29% of observed heavy precipitation anomaly over SGP in the WRF simulation (Figure 6a). Table 2 summarizes the results from these three experiments. The results for the LST/SUBT effects are quite consistent in the model simulation; for every ensemble member pair, the case with imposed positive SUBT anomaly produced large precipitation than the case without the imposed SUBT anomaly, with the standard deviation being

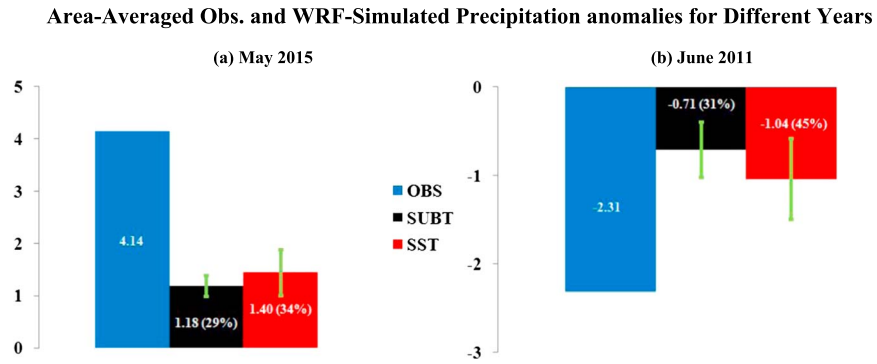

Figure 6. Observed and simulated precipitation anomalies over United States. (a) Area-averaged observed and WRF simulated (LST and SUBT and SST effects) May 2015 precipitation anomalies over SGP (88–103°W and 29–38°N). (b) Area-averaged observed and WRF simulated (LST and SUBT and SST effects) June 2011 precipitation deficit over SGP. The bars show the standard deviation of ensemble members. Units: Precipitation: mm/day.

Table 2
Observed and WRF Simulated May 2015 Precipitation and Differences (Units: mm/day) for Different Scenarios Averaged Over the SGP, as Identified in Figure 4a by the Box

GTS observations		WRF-simulated precipitation		
May 2015	Reference for the May 2015 case	Case 2015_NA (CTRL)	Case noSUBT_NA	Case noSST_NA
7.617	3.477	4.630	3.444	3.230
		Differences of CTRL and different cases		
GTS difference of May 2015 and reference		CTRL minus case noSUBT_NA	CTRL minus case noSST_NA	
4.140		1.186 (28.6%)	1.400 (33.8%)	

Note. The percentages in parentheses were derived from the ration between the difference of CTRL and different cases and the difference of May 2015 observation and reference.

0.21 mm/day. We only show the WRF results in Figure 6 because WRF produces better regional anomaly. For comparison, the SST effect is shown in Figures 5d and 5e. SST produced statistically significant wet condition along southern coastal states and contributed to about 34% of observed precipitation anomalies in the WRF simulations, with standard deviation being 0.44 mm/day (Figure 6a); however, the wet conditions in eastern coastal areas were not consistent with observed anomalies. The sum of these two effects is slightly less than two thirds of the observed anomaly. For comparison, Figure 6b also shows the results of our 2011 SGP drought study (Xue, Oaida, et al., 2016). In that study, cold LST and SUBT in WUS in spring contributed to about 31% of precipitation anomaly (drought) in the WRF modeling results, while the SST effect was higher compared to the 2015 flood case (~45%). The ratios of LST/SUBT effect and SST effect, which may be less affected by the model bias, for 2015 Case and 2011 Case were 0.85 and 0.69, respectively. The assessments for different effects here are preliminary and affected by the model systematic errors. Multimodel approach is necessary to make a more realistic assessment as we did in the Second West African Monsoon Modeling and

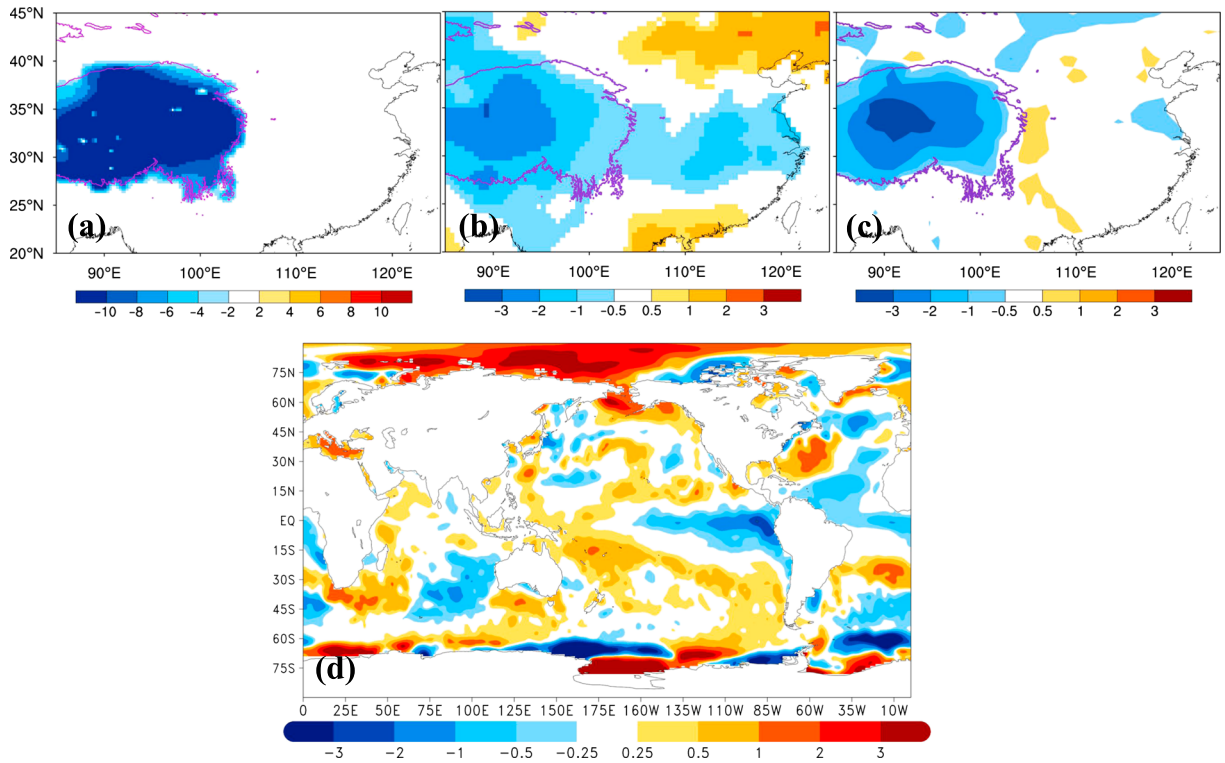

Figure 7. (a) Imposed subsurface temperature (SUBT) difference over TP at the first time step of the model simulation between Case 2003_EA and Case noSUBT_EA. (b) Observed May 2 m-temperature (T2 m) anomaly between 2003 and the reference. (c) GFS-simulated May T2 m difference between Case 2003_EA and Case noSUBT_EA. (d) May 2003 SST difference between Case 2003_EA and Case noSST_EA. Unit: °C.

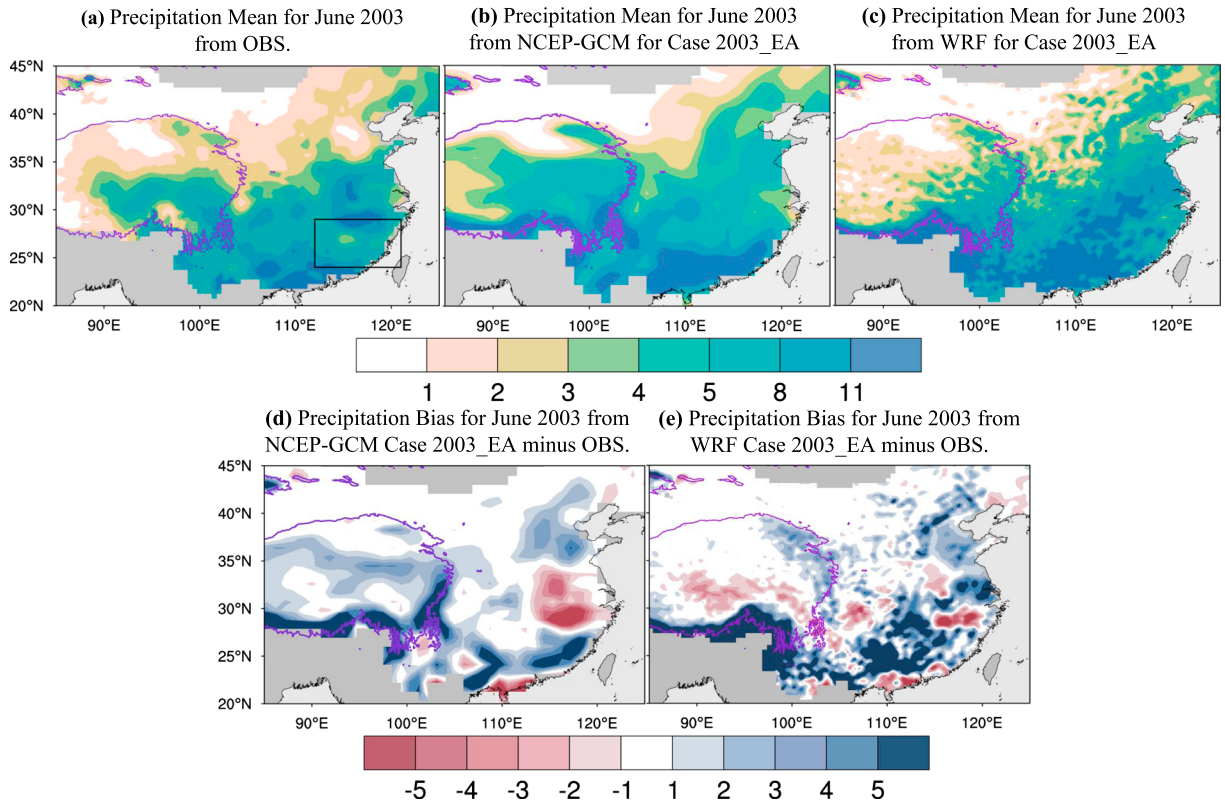

Figure 8. Mean precipitation for (a–c) June 2003 and (d and e) mean biases over East Asia. (a) Observations, (b) NCEP-GFS simulations (GFS Case 2003_EA), and (c) WRF-NMM simulations (WRF Case 2003_EA). (d and e) are mean biases with respect to OBS from Case 2003_EA of NCEP-GCM and WRF, respectively. Box in (a) indicates the southern Yangtze River basin used for precipitation regional averages. Unit: mm/day.

Evaluation experiment (Xue, De Sales, et al., 2016). In addition to these two factors, other elements such as atmospheric internal variability (Seager et al., 2014), soil moisture (Koster et al., 2004, 2014, 2016; Sun et al., 2015), and vegetation (Xue et al., 1996, 2010) conditions may also contribute to the observed anomaly.

Using the observed T2 m anomaly as a constraint, the numerical experiments here have confirmed the contribution of the LST/SUBT anomaly in WUS on the 2015 flood in SGP. Consistent with our previous 2011 SGP drought study (Xue, Oaida, et al., 2016), its effect in SGP is comparable with the SST effect. In the next section, we further demonstrate that this approach may also be useful for other areas, that is, the East Asia, which has a similar geographic setting.

3.2. The 2003 East Asian Drought/Flood

3.2.1. Brief Background

The 2003 summer and fall seasons were characterized by a severe drought over the southern part of the Yangtze River in eastern China, which resulted in 100×10^6-kg crop yield losses, mostly rice, but also cotton, wheat, barley, corn, beans, and hemp, along with an economic loss of 5.8 billion Chinese Yuan (Zhang & Zhou, 2015). To the north of the Yangtze River, there was above normal precipitation (Seol & Hong, 2009) with relative less area (see Figure 9a). Meanwhile, Chinese observational data show that there was a cold spring in the TP. The average T2 m difference in April–May between the year 2003 and the average of the 5 years with warmest T2 m (i.e., years 1994, 1995, 1998, 2008, and 2010) over the TP area (25–40°N and 85–105°E with elevations above 2,500 m) was −2.03°C. This 2003 anomaly in East Asia was not as strong as the 2015 North American case but covered a larger area.

3.2.2. Experimental Design

Similar to the North American study, three cases were designed for the East Asian study. Each case was integrated for 2 months from 27 April to 30 June 2003 with eight ensemble members. In GFS Case 2003_EA, the 2003 atmospheric and land data from the reanalysis of the Climate Forecast System were used as initial

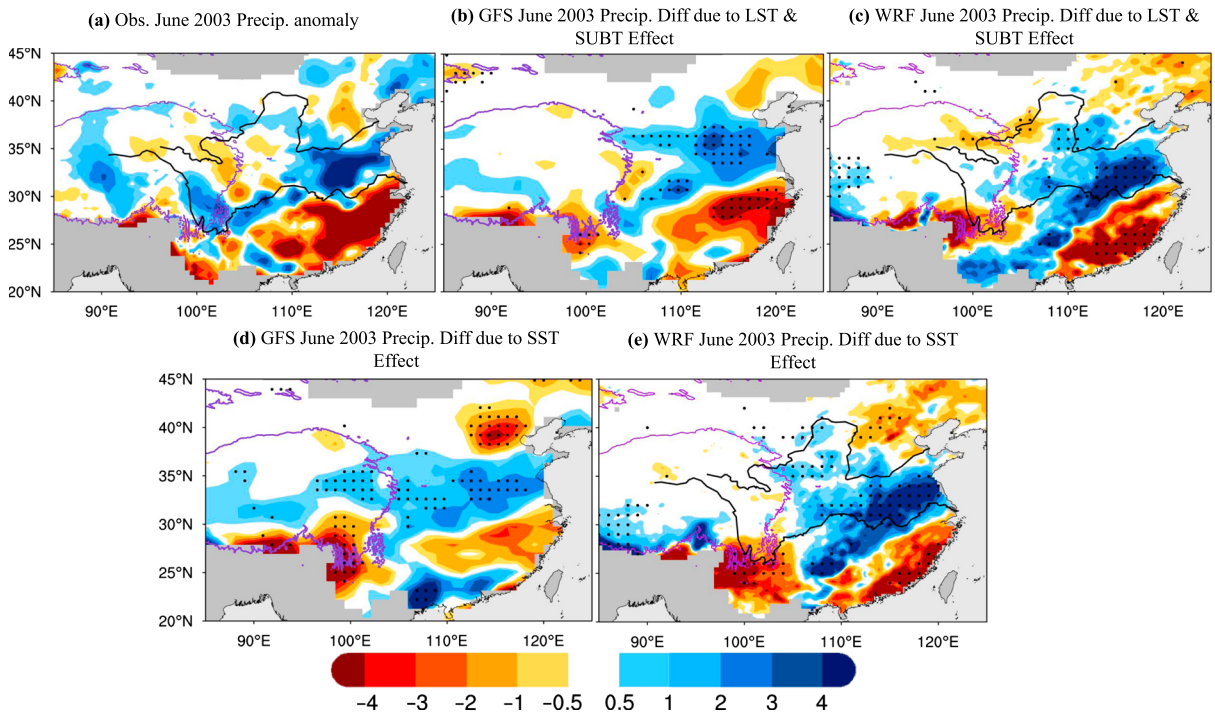

Figure 9. Observed and simulated June 2003 precipitation anomalies over East Asia. (a) Observed June precipitation difference between 2003 and the reference; (b) GFS-simulated precipitation difference due to LST and SUBT effect; (c) same as (b) but for WRF; (d) GFS-simulated precipitation difference due to SST effect; and (e) same as (d) but for WRF. Units: mm/day. The stippled areas denote the statistical significance at the $\alpha < 0.1$ level of *t* test values. The gray shaded areas indicate no observational data.

conditions (Saha et al., 2010), and observed 2003 SST and sea ice data were used as boundary conditions for GFS. For the similar reasons as discussed in section 3.1.2, in GFS Case 2003_EA, the control case, we imposed the cold LST and SUBT anomalies at the first time step of the model simulation over TP based on the observed T2 m difference between April 2003 and the April mean of 1981–2015 but with tuning (Figure 7a) and aimed to reproduce the observed May T2 m negative anomaly over the TP (Figures 7b and 7c). Since the GFS and WRF had wet bias over the eastern part of China, this setting would make the model simulation dry, which is similar to our discussions in section 3.1.2, in which we had to impose initial warm LST and SUBT in the control case to be able to produce the wet conditions over SGP. The WRF initial and LBC were obtained from the corresponding NCEP-GFS cases. Case 2003_EA produced observed June monsoon precipitation to the south of 35°N, but still with a wet bias for the WRF run even after imposing the initial cold TP temperature (Figure 8). The June precipitation average over the eastern part of China (112–121°E and 24–35°N) was 7.06, 6.69, and 9.09 mm/day for observation, GFS, and WRF, respectively. Although the WRF produced a wet bias, it produced the observed precipitation center along the Yangtze River around 30°N. Both models reproduced observed heavy precipitation along the southern coastal area of the East Asia; but the monsoon rain was extended much to the north of 35°N (Figure 8). The second experiment, GFS Case noSUBT_EA, is the same as GFS Case 2003_EA, except that the cold LST and SUBT were not imposed on the first time step of the model simulations.

As discussed in section 3.1.2, we had to evaluate the simulated May T2 m difference between Case 2003_EA and Case noSUBT_EA and compared with the observed T2 m anomaly to decide which reference is proper to assess the LST/SUBT effect and to test the SST effect. The T2 m difference over TP between GFS Case 2003_EA and GFS Case noSUBT_EA (−1.78 °C) is closer to the observed difference (−1.63 °C) between May 2003 and the mean of five extreme warm years (1994, 1995, 1998, 2008, and 2010; Figures 7b and 7c) than to that between the May 2003 surface temperature and climatology (−0.86 °C). Since we used the simulated T2 m difference over TP (−1.78 °C) as a constraint to compare the simulated LST/SUBT effect with the observation and the SST effect, in this case we used the extreme years mean as the reference as did in previous studies (Xue, Oaida, et al., 2016; Xue et al., 2012). In the third experiment, GFS Case noSST_EA, the reference daily

Table 3
SST and Initial SUBT Conditions for Different East Asian Cases

Cases	Initial SUBT conditions	SST boundary conditions	Note
Case 2003_EA	Imposing anomaly. Figure 7a	2003 SST	East Asian control (CTRL) case
Case noSUBT_EA	No imposed anomaly	2003 SST	East Asian control case minus this case shows SUBT effect.
Case noSST_EA	Same as case 2003_EA	Reference SST	East Asian control case minus this case shows SST effect.

SST, that is, the mean SST of the five warm years (1994, 1995, 1998, 2008, and 2010) was used to replace the 2003 SST conditions. The May SST difference between GFS Case 2003_EA and GFS Case noSST_EA is shown in Figure 7d. Overall, the most notable SST difference between these two cases was the La Niña feature in the Pacific Ocean. A MCA analysis had shown that the SST El Niño–Southern Oscillation pattern is significantly associated with precipitation variability over China (Xue et al., 2005). Based on the experimental design, the only difference between Case 2003_EA and Case noSUBT_EA (Figures 9b and 9c) and the difference between Case 2003_EA and Case noSST_EA (Figures 9d and 9e) were due to difference in the LST/SUBT and SST, respectively, and were used to assess each impact on the EA drought/flood condition due to these respective factors. These experiments are listed in Table 3, and a detailed discussion of these results is presented in the following section.

3.2.3. LST/SUBT Effects

Figure 9a shows the observed precipitation difference between June 2003 and the reference. Table 4 summarizes the WRF results for area-averaged precipitation over the southern Yangtze River from the three experiments. The observed anomaly shows a severe drought (a reduction of 6.04 mm/day, Figure 10) over the region south of the Yangtze River and wet condition to the north. The LST and SUBT effect in the GFS and WRF simulations produced statistically significant dry conditions over some areas to the south of the Yangtze River (Figures 9b and 9c). The boundary of dry and wet regions along the Yangtze River was very nicely reproduced in the GFS. However, the wet and normal precipitation area along the China's southern coastal area in the GFS simulation was inconsistent with the observed drought there. On the other hand, the WRF reproduces the drought to the south of the Yangtze River very well; the area with positive precipitation anomaly, however, was larger than observed and extended to the south. The LST/SUBT effect produced about 62% of observed drought condition by the WRF (Figure 10). The SST effect by the WRF also produced a statistically significant dipole anomaly pattern of precipitation (Figure 9e) and produced about 38% of the drought conditions to the south of the Yangtze River (Figure 10). The drought area with statistical significance was much smaller than that produced by the LST/SUBT effect, and the wet area extended farther to the south in the WRF simulation. In the East Asian case, the standard deviation for the SUBT and SST effects as shown in Figure 10 were 2.02 and 0.85 mm/day, respectively. The sum of these two factors produced total observed precipitation anomaly, higher than in the North American case, which may be partially due to the wet bias in the control cases (see Figures 8d and 8e). Nevertheless, this case study confirms that both LST and SST play a role in East Asian drought/flood. Different from the North American case, the TP LST anomaly seems to play

Table 4
Observed and WRF Simulated June 2003 Precipitation and Differences (Units: mm/day) for Different Scenarios Averaged Over the Southern Yangtze River Region as Highlighted in Figure 8a by the Box

GTS observations		WRF-simulated precipitation		
June 2003	Reference for the June 2003 case	Case 2003_EA (CTRL)	Case noSUBT_EA	Case noSST_EA
6.649	12.685	9.805	13.565	12.116
		Differences of CTRL and different cases		
GTS difference of June 2003 and reference		CTRL minus case noSUBT_EA	CTRL minus case noSST_EA	
−6.036		−3.757 (−62.24%)	−2.311 (−38.29%)	

Note. The percentages in parentheses were derived from the ration between the difference of CTRL and different cases and the difference of June 2003 observation and reference.

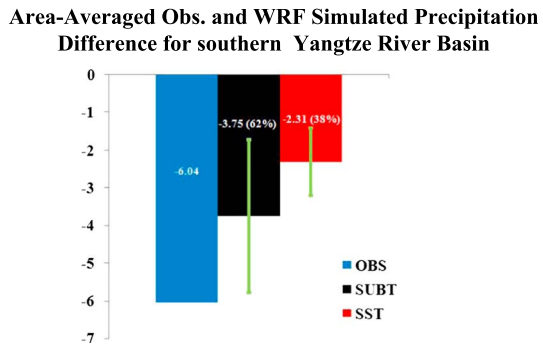

Figure 10. Area-averaged of observed and simulated (LST and SUBT and SST effects) June 2003 precipitation deficit over southern Yangtze River basin (24–29°N, 112–121°E). The bars show the standard deviation of ensemble members. Units: mm/day.

a more robust role in the rainfall anomaly over East Asia compared to SST anomalies; the ratio of LST/SUBT effect and SST effect for this East Asia case is 1.63. More case studies are necessary to assess the relative contributions from these two factors, as well as contributions from other factors further.

3.3. Mechanisms

The possible mechanisms of LST and SUBT effects in North America have been explored in early studies (Xue, Oaida, et al., 2016; Xue et al., 2012). Here we further delineate the mechanisms and summarize the main processes in North America. Figure 11a shows average sensible heat flux difference between GFS Case 2015_NA and GFS Case noSUBT_NA for the first 2 weeks of the simulation (positive values indicate an upward flux). The initial imposed warm LST/SUBT in the WUS generated a positive sensible heat flux anomaly, which in turns produced a positive geopotential height anomaly aloft (Figure 11b). The WRF simulations have very similar results (not shown). The impact of LST anomaly in the West U.S. is transmitted through the atmosphere through large-scale Rossby wave motions (Figure 12). Figure 12 shows the simulated 500-hPa geopotential height differences between Case 2015_NA and Case noSUBT_NA for GFS (top panels) and WRF (bottom panels). The WRF adequately downscaled the GFS wave train across the North American continent (Figures 12d–12df). The warm temperature anomaly in the West heats the surface and low and middle troposphere and produces an anomalous positive geopotential height in the middle troposphere (Figure 11b), inducing an anomalous planetary wave train across North America, especially in week 1–2 (Figures 12a and 13). This pattern may be compared to the well-known Pacific-North American pattern that is associated with both SST teleconnections (Hoerling et al., 2014; Trenberth et al., 1988) and atmospheric internal variability (Wallace & Gutzler, 1981). The pattern in Figure 12a has qualitative similarities to the Pacific-North American's but differs in the location and extent of the geopotential anomaly highs and lows, consistent with the LST effect, thus providing an independent contribution via similar Rossby wave dynamics. Although the geopotential height anomaly over the North American continent shows a general stationary pattern, the negative geopotential height anomaly in eastern North America grows and extends to the south during weeks 3–4 and weeks 5–6 (i.e., first half of May), associated with strong positive vorticity and anomalous cyclonic circulation (Figures 12c and 12f), leading to heavy precipitation. This study aimed to isolate the LST/SUBT mechanism (Figures 12 and 13). It should be pointed out that to be comparable with the observation, both LST/SUBT and SST effects should be considered as did for the precipitation.

The above analyses show that the LST downstream effects are associated with a large-scale atmospheric stationary wave extending eastward from the LST anomaly region. This process is summarized in the schematic diagram (Figure 13). It has been previously noted that 500-hPa climatological mean geopotential stationary

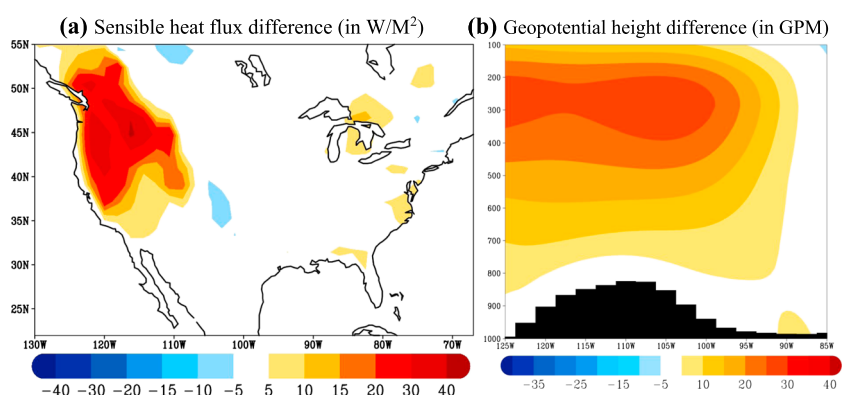

Figure 11. NCEP-GFS simulated difference between Case 2015_NA and Case noSUBT_NA for the first 2 weeks of April: (a) sensible heat flux at the surface (W/m^2) and (b) geopotential height (GHT, in GPM) averaged between 33°N and 50°N. Black area in (b) indicates topography.

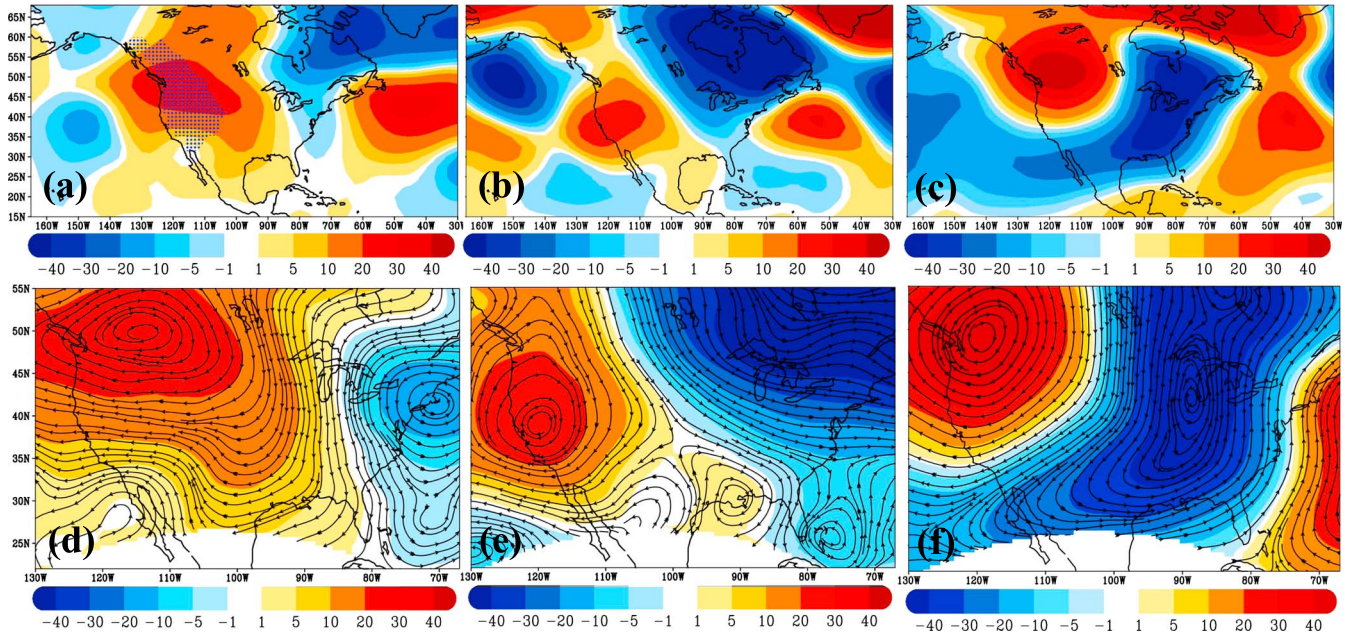

Figure 12. Sequence for LST anomaly-induced wave trains, April through mid-May. (a–c) NCEP-GFS simulated 500-hPa geopotential height (GPM) differences due to LST/SUBT effect for weeks 1–2, weeks 3–4, and weeks 5–6, respectively. (d–f) Same as (a–c) but for WRF simulations, with superimposed wind streamlines due to LST and SUBT effects. Stippled area in (a) represents the region with imposed LST and SUBT at the first step of the model integration.

wave pattern in late spring and early June has its troughs over the east and west coasts of the U.S. and its broad ridge extends from the Rocky Mountains eastward to the Great Lakes (Figure 14; Chang & Wallace, 1987). This climate feature favors a southward steering flow, helping the negative geopotential height anomaly/positive vorticity to extend to the south in the North American case (Figures 12b, 12c, 12e, 12f, and 13; Xue et al., 2012). As soon as the positive vorticity anomaly reaches the Gulf of Mexico, abundant moisture and convective instability and condensation heating favored a strong positive feedback to support

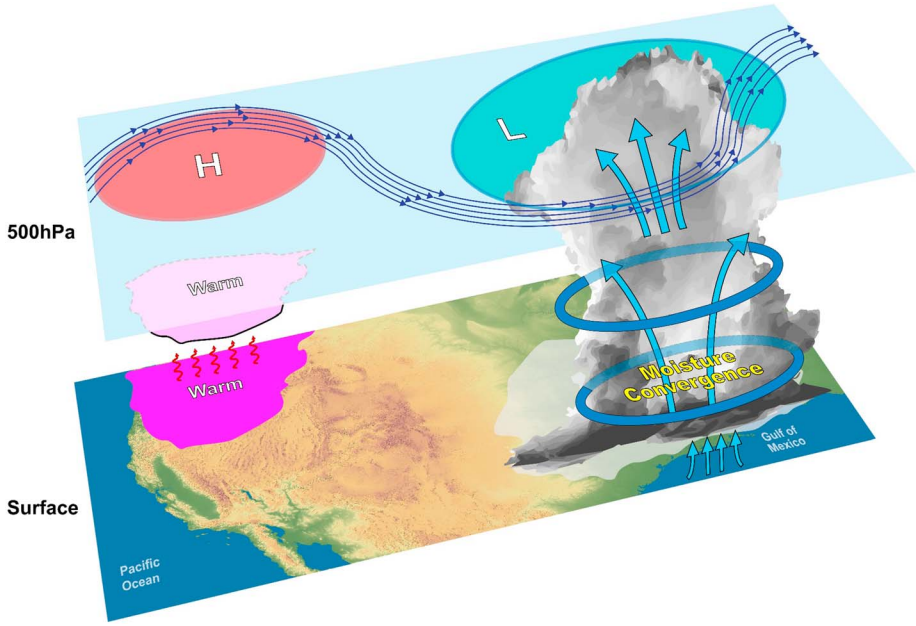

Figure 13. Schematic diagram describing the processes associated with the impact of LST and SUBT anomalies affecting downstream precipitation.

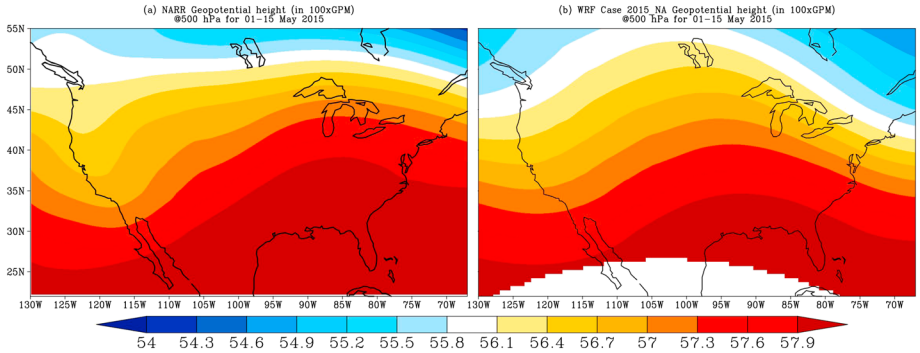

Figure 14. The 1–15 May 2015 geopotential height at 500 hPa from (a) NARR reanalysis and (b) WRF Case 2015_NA. Unit: 10^2 GPM.

the convective activity there by itself, which may contribute to the growth of a strong cyclonic system (Figures 12c, 12f, and 13).

The local response due to the LST/SUBT effect for the East Asian case is similar to the North American case. For instance, the cold temperature over TP in our 2003 case produced negative sensible heat flux and geopotential height anomalies over the TP (Figure S6). The interaction process, however, is quite complex in East Asia and different from the North America because these two continents have quite different regional climate systems. One of the important climate features in East Asia is the South Asian High (SAH; also called the Tibetan High), which is a planetary-scale anticyclonic circulation system in the upper troposphere, with its main part located over the TP and neighboring areas during late spring and summer (e.g., Liu et al., 2013). The SAH exhibits subseasonal zonal oscillation, which, especially its eastern extension, contributes to Asian monsoon variability (e.g., Jia & Yang, 2013; Yuan et al., 2012). This oscillation has been attributed to the modulation induced by diabatic heating from precipitation and influences of the midlatitudes wave train over the Eurasian continent (e.g., Ding & Wang, 2007; Fujinami & Yasunari, 2004; Wu et al., 2012). It has been suggested that these two mechanisms work together to give rise to the zonal oscillation of the SAH at intraseasonal time scales and then to summer precipitation (Ren et al., 2015). We conjecture that LST/SUBT anomaly-induced diabatic heating in the TP would interact with the midlatitudes wave train and SAH, influencing East Asian monsoon precipitation variability. The East Asian LST/SUBT research is still in the preliminary stage. More comprehensive investigations are necessary to better understand the mechanisms and investigate our hypothesis.

4. Conclusion

While numerous studies have focused on the teleconnection between SST anomalies and droughts/floods, the remote effect of large-scale LST anomalies in geographical areas upstream and closer to the areas of extreme drought and flood has largely been ignored. Based on analyses of observational data and modeling studies, this study and our previous studies (Xue, Oaida, et al., 2016; Xue et al., 2012) suggest a new mechanism that may contribute to drought/flood events in the North American and East Asian continents. It is found that cold (warm) spring LST in the high elevation areas of WUS and TP may contribute to the drought (flood) downstream, namely, in the SGP in the U.S. and lowland plain in eastern China. Consideration of both SST and LST anomalies is able to explain a substantial amount of variance in precipitation at intraseasonal and seasonal scales and provides a practical and more reliable means to predict dry and wet conditions, in particular extreme drought/flood events. It is likely that when the LST/SUBT and SST anomalies work in the same direction, extreme events occur as found in this and other studies (Xue, De Sales, et al., 2016; Xue, Oaida, et al., 2016). Although this study focuses on two regions, it would motivate testing those relationship and general physical principles and mechanisms in other regions with similar geographic settings.

While the results here make the case for LST downstream impact, in particular hydroclimate circumstances, questions remain that motivate further investigations. One such question is the initial cause for the large-scale LST/SUBT anomaly, especially its relationship with snow, SST, soil moisture, and others. Our previous study (Xue, Oaida, et al., 2016) indicated that LST anomalies in WUS and SST anomalies only had moderate correlations and the years in which both exhibited extreme values were not always concurrent. Recent

studies (Koster et al., 2016, 2014) have suggested that the enforced atmospheric diabatic heating and soil moisture could induce precipitation and surface temperature anomalies over different regions through teleconnection. We have conjectured that LST/SUBT anomalies have a temporally filtered contribution from preceding snow anomalies. The causes of the LST/SUBT anomalies need to be further investigated but may require more observational data on this aspect and substantial modeling investment in the subsurface processes that yield memory of deep soil temperature. Our numerical studies examine the effects of LST/SUBT anomalies with 1 month lead, but it remains an open question whether longer lead time could exhibit potential predictability.

The role of SST in climate variability has been studied for several decades. The study of the LST effects from high elevation areas on downstream regions is still in its incipient stages, which challenges the modeling community to simulate the land surface heating-atmosphere interactions and land-induced wave train in the atmosphere properly and to simulate the memory of deep soil temperature adequately. More research with different cases, different models, and different experimental designs are necessary to further test this hypothesis. Our LST/SUBT studies (e.g., Xue, Oaida, et al., 2016; Xue et al., 2012) and other studies (e.g., Koster et al., 2014, 2016) suggest that the effect of land/atmosphere interaction through modulating the planetary wave is a subject worth further research.

One issue that hampers the application for this LST/SUBT approach for the intraseasonal to seasonal prediction is data availability. Large-scale LST and SUBT data are still lacking. The reanalysis surface variables (including the rainfall, snow, soil temperature, and soil moisture) were all reanalysis systems land model products. A number of studies have pointed out problems, especially biases, in reanalysis surface products (e.g., Xue et al., 2001, 2007; Higgins et al., 2010; Broxton et al., 2016). In particular, problems with precipitation (rain and snow) affect surface water and energy balances as much as if not more than soil temperature and other soil variables. Figure S7 in the supporting information shows the normalized (i.e., removal of the soil column mean of soil temperatures) May TP soil temperature profiles from three observational stations (Yang & Zhang, 2016) and from the reanalysis over these sites. The observation shows that the temperature warms at the surface then cools down until about 1.5 m then it warms again, a sign of the memory from previous months. The CFSR shows a straight cooling from the surface to 2 m in the soil. Moreover, the CAMS and NMIC (2012) show that the mean May surface temperature over TP in 2003 was 1.2 °C, a cold year as mentioned before. The CFSR data show that the May 2003 TP surface temperature was 4.59 °C, a quite warm year. Special caution has to be taken when employing the reanalysis land products for the LST/SUBT study. We postulate that after further development and improvements in land models and LST and SUBT data regarding these processes, and comprehensive understanding the causes of land memory, this LST/SUBT approach will provide a useful tool for addressing drought and flood prediction issues with broad societal impacts.

Acknowledgments
This work was supported by the grants from U.S. National Science Foundation AGS-1346813, AGS-1419526, and AGS-1540518 (J. D. N.). This work is also supported by the Jiangsu Collaborative Innovation Center for Climate Change, China. The authors thank Professor Jared Diamond of UCLA for his comments and contributions to the manuscript revisions. We also appreciate Mr. Matt Zebrowski, Miss Huilin Huang of UCLA, and Dr. Wei Li of NCEP's technical assistance with this article. The three anonymous reviewers have very carefully reviewed the manuscript and provided insightful, constructive, critical, and encouraging comments and suggestions. We sincerely appreciate their great efforts. The CAMS gridded 2-m temperature is available at https://www.esrl.noaa.gov/psd/data/gridded/data.ghcncams.html. The CPC daily precipitation is available at https://www.esrl.noaa.gov/psd/thredds/catalog/Datasets/cpc_us_precip/catalog.html. The China Ground 2-m Temperature and Precipitation Grid Dataset is available at http://cdc.nmic.cn. The simulation data used for this paper are available at https://ucla.box.com/s/9yzkqk7bf2281g41flxrfyczy2ues50f.

References

Bamzai, A. S., & Shukla, J. (1999). Relation between Eurasian snow cover, snow depth, and the Indian summer monsoon: An observational study. *Journal of Climate*, *12*(10), 3117–3132. https://doi.org/10.1175/1520-0442(1999)012%3C3117:RBESCS%3E2.0.CO;2

Barlow, M., Nigam, S., & Berbery, E. H. (2001). ENSO, Pacific decadal variability, and US summertime precipitation, drought, and stream flow. *Journal of Climate*, *14*(9), 2105–2128. https://doi.org/10.1175/1520-0442(2001)014%3C2105:EPDVAU%3E2.0.CO;2

Barsugli, J. J., & Battisti, D. S. (1998). The basic effects of atmosphere-ocean thermal coupling on mid-latitude variability. *Journal of Atmospheric Science*, *55*(4), 477–493. https://doi.org/10.1175/1520-0469(1998)055%3C0477:TBEOAO%3E2.0.CO;2

Broxton, P. D., Zeng, X., & Dawson, N. (2016). Why do global reanalyses and land data assimilation products underestimate snow water equivalent? *Journal of Hydrometeorology*, *17*(11), 2743–2761. https://doi.org/10.1175/JHM-D-16-0056.1

Chang, F. C., & Wallace, J. M. (1987). Meteorological conditions during heat waves and droughts in the United States Great Plains. *Monthly Weather Review*, *115*(7), 1253–1269. https://doi.org/10.1175/1520-0493(1987)115%3C1253:MCDHWA%3E2.0.CO;2

Chen, M., Xie, P., Janowiak, J. E., & Arkin, P. A. (2002). Global land precipitation: A 50-yr monthly analysis based on gauge observations. *Journal of Hydrometeorology*, *3*(3), 249–266. https://doi.org/10.1175/1525-7541(2002)003%3C0249:GLPAYM%3E2.0.CO;2

Deardorff, J. W. (1978). Efficient prediction of ground surface temperature and moisture, with inclusion of a layer of vegetation. *Journal of Geophysical Research*, *83*(C4), 1889–1903. https://doi.org/10.1029/JC083iC04p01889

Dey, B., & Bhanu Kumar, O. S. R. U. (1983). Himalayan winter snow covers area and summer monsoon rainfall over India. *Journal of Geophysical Research*, *88*(C9), 5471–5474. https://doi.org/10.1029/JC088iC09p05471

Dickinson, R. E. (1988). The force-restore model for surface temperatures and its generalizations. *Journal of Climate*, *1*(11), 1086–1097. https://doi.org/10.1175/1520-0442(1988)001%3C1086:TFMFST%3E2.0.CO;2

Ding, Q., & Wang, B. (2007). Intraseasonal teleconnection between the summer Eurasian wave train and the Indian monsoon. *Journal of Climate*, *20*(15), 3751–3767. https://doi.org/10.1175/JCLI4221.1

Entin, J. K., Robock, A., Vinnikov, K. Y., Hollinger, S. E., Liu, S., & Namkhai, A. (2000). Temporal and spatial scales of observed soil moisture variations in the extratropics. *Journal of Geophysical Research*, *105*(D9), 11,865–11,877. https://doi.org/10.1029/2000JD900051

Fan, Y., & Van den Dool, H. (2008). A global monthly land surface air temperature analysis for 1948-present. *Journal of Geophysical Research*, *113*, D01103. https://doi.org/10.1029/2007JD008470

Fujinami, H., & Yasunari, T. (2004). Submonthly variability of convection and circulation over and around the Tibetan Plateau during the boreal summer. *Journal of the Meteorological Society of Japan*, *82*(6), 1545–1564. https://doi.org/10.2151/jmsj.82.1545

Groisman, P. Y., Knight, R. W., Karl, T. R., Easterling, D. R., Sun, B., & Lawrimore, J. H. (2004). Contemporary changes of the hydrological cycle over the contiguous United States: Trends derived from in situ observations. *Journal of Hydrometeorology*, *5*(1), 64–85. https://doi.org/10.1175/1525-7541(2004)005%3C0064:CCOTHC%3E2.0.CO;2

Higgins, R. W., Kousky, V. E., Silva, V. B. S., Becker, E., & Xie, P. (2010). Intercomparison of daily precipitation statistics over the United States in observations and in NCEP reanalysis products. *Journal of Climate*, *23*(17), 4637–4650. https://doi.org/10.1175/2010JCLI3638.1

Hoerling, M., Eischeid, J., Kumar, A., Leung, R., Mariotti, A., Mo, K., et al. (2014). Causes and predictability of the 2012 Great Plains drought. *Bulletin of the American Meteorological Society*, *95*(2), 269–282. https://doi.org/10.1175/BAMS-D-13-00055.1

Hu, Q., & Feng, S. (2004). A role of the soil enthalpy in land memory. *Journal of Climate*, *17*(18), 3633–3643. https://doi.org/10.1175/1520-0442(2004)017%3C3633:AROTSE%3E2.0.CO;2

Huang, R., Chen, J., & Huang, G. (2007). Characteristics and variations of the East Asian monsoon system and its impacts on climate disasters in China. *Advances in Atmospheric Sciences*, *24*(6), 993–1023. https://doi.org/10.1007/s00376-007-0993-x

Janjic, Z., Black, T., Pyle, M., Ferrier, B., Chuang, H. Y., Jovic, D., et al. (2011). User's guide for the NMM core of the weather research and forecast (WRF) modeling system version 3 (p. 195). (http://dtcenter.org/wrf-nmm/users/) developmental testbed center/National Centers for Environmental Prediction, Boulder (p. 213).

Jia, X., & Yang, S. (2013). Impact of the quasi-biweekly oscillation over the western North Pacific on East Asian subtropical monsoon during early summer. *Journal of Geophysical Research*, *118*, 4421–4434. https://doi.org/10.1002/jgrd.50422

Kanamitsu, M., Ebisuzaki, W., Woollen, J., Yang, S.-K., Hnilo, J. J., Fiorino, M., & Potter, G. L. (2002). NCEP–DOE AMIP-II Reanalysis (R-2). *Bulletin of the American Meteorological Society*, *83*(11), 1631–1644. https://doi.org/10.1175/BAMS-83-11-1631

Karl, T. R., Groisman, P. Y., Knight, R. W., & Heim, R. R. Jr. (1993). Recent variations of snow cover and snowfall in North America and their relation to precipitation and temperature variations. *Journal of Climate*, *6*(7), 1327–1344. https://doi.org/10.1175/1520-0442(1993)006%3C1327:RVOSCA%3E2.0.CO;2

Koster, R. D., Chang, Y., & Schubert, S. D. (2014). A mechanism for land-atmosphere feedback involving planetary wave structures. *Journal of Climate*, *27*(24), 9290–9301. https://doi.org/10.1175/JCLI-D-14-00315.1

Koster, R. D., Chang, Y., Wang, H., & Schubert, S. D. (2016). Impacts of local soil moisture anomalies on the atmospheric circulation and on remote surface meteorological fields during boreal summer: A comprehensive analysis over North America. *Journal of Climate*, *29*(20), 7345–7364. https://doi.org/10.1175/JCLI-D-16-0192.1

Koster, R. D., Dirmeyer, P. A., Guo, Z., Bonan, Z., Chan, E., Cox, P., et al. (2004). Regions of strong coupling between soil moisture and precipitation. *Science*, *305*(5687), 1138–1140. https://doi.org/10.1126/science.1100217

Leathers, D. J., & Robinson, D. A. (1993). The association between extremes in North American snow cover extent and United States temperatures. *Journal of Climate*, *6*(7), 1345–1355. https://doi.org/10.1175/1520-0442(1993)006%3C1345:TABEIN%3E2.0.CO;2

Liu, B., Wu, G., Mao, J., & He, J. (2013). Genesis of the South Asian high and its impact on the Asian summer monsoon onset. *Journal of Climate*, *26*(9), 2976–2991. https://doi.org/10.1175/JCLI-D-12-00286.1

Liu, X. D., & Yanai, M. (2002). Influence of Eurasian spring snow covers on Asian summer rainfall. *International Journal of Climatology*, *22*(9), 1075–1089. https://doi.org/10.1002/joc.784

Mahanama, S. P. P., Koster, R. D., Reichle, R. H., & Suarez, M. J. (2008). Impact of subsurface temperature variability on surface air temperature variability: An AGCM study. *Journal of Hydrometeorology*, *9*(4), 804–815. https://doi.org/10.1175/2008JHM949.1

Mekonnen, A., Renwick, J. A., & Sánchez-Lugo, A. (Eds) (2016). Regional climates in "State of the climate in 2015". *Bulletin of the American Meteorological Society*, *97*(8), S173–S226.

Mo, K. C., Schemm, J. K. E., & Yoo, S. H. (2009). Influence of ENSO and the Atlantic multidecadal oscillation on drought over the United States. *Journal of Climate*, *22*(22), 5962–5982. https://doi.org/10.1175/2009JCLI2966.1

National Meteorological Information Center (NMIC) (2012). *Assessment report of China's Ground Precipitation 0.5°×0.5° Gridded Dataset (V2.0)* [in Chinese]. Beijing*: National Meteorological Information Center*.

Palmer, T. N. (1986). Influence of the Atlantic, Pacific and Indian Oceans on Sahel rainfall. *Nature*, *322*(6076), 251–253. https://doi.org/10.1038/322251a0

Pu, B., Fu, R., Dickinson, R. E., & Fernando, D. N. (2016). Why do summer droughts in the Southern Great Plains occur in some La Niña years but not others? *Journal of Geophysical Research: Atmosphere*, *121*, 1120–1137. https://doi.org/10.1002/2015JD023508

Ren, X., Yang, D., & Yang, X.-Q. (2015). Characteristics and mechanism of sub-seasonal eastward extension of South Asian high. *Journal of Climate*, *28*(17), 6799–6822. https://doi.org/10.1175/JCLI-D-14-00682.1

Robinson, D. A. (2015). The 2014–2015 U.S. snow report: The northeast steals the snow. *Weatherwise*, *68*(6), 20–29. https://doi.org/10.1080/00431672.2015.1086239

Robock, A., Mu, M., Vinnikov, K., & Robinson, D. (2003). Land surface conditions over Eurasia and Indian summer monsoon rainfall. *Journal of Geophysical Research*, *108*(D4), 4131. https://doi.org/10.1029/2002JD002286

Ropelewski, C. F., Jonowiak, J. E., & Halper, M. E. (1985). The analysis and display of real time surface climate data. *Monthly Weather Review*, *113*(6), 1101–1106. https://doi.org/10.1175/1520-0493(1985)113%3C1101:TAADOR%3E2.0.CO;2

Rui, M., & Wang, G. (2011). Impact of sea surface temperature and soil moisture on summer precipitation in the United States based on observational data. *Journal of Hydrometeorology*, *12*(5), 1086–1099.

Saha, S., Moorthi, S., Pan, H. L., Wu, X., Wang, J., Nadiga, S., et al. (2010). The NCEP climate forecast system reanalysis. *Bulletin of the American Meteorological Society*, *91*(8), 1015–1058. https://doi.org/10.1175/2010BAMS3001.1

Scaife, A. A., Kucharski, F., Folland, C. K., Kinter, J., Bronnimann, S., Fereday, D., et al. (2009). The CLIVAR C20C project: Selected 20th century climate events. *Climate Dynamics*, *33*(5), 603–614. https://doi.org/10.1007/s00382-008-0451-1

Schubert, S., Gutzler, D., Wang, H., Dai, A., Delworth, T., Deser, C., et al. (2009). A U.S. CLIVAR project to assess and compare the responses of global climate models to drought-related SST forcing patterns: Overview and results. *Journal of Climate*, *22*(19), 5251–5272. https://doi.org/10.1175/2009JCLI3060.1

Seager, R., Goddard, L., Nakamura, J., Henderson, N., & Lee, D. E. (2014). Dynamical causes of the 2010/11 Texas–northern Mexico drought. *Journal of Hydrometeorology*, *15*(1), 39–68. https://doi.org/10.1175/JHM-D-13-024.1

Sellers, P. J., Randall, D. A., Collatz, G. J., Berry, J. A., Field, C. B., Dazlich, D. A., et al. (1996). A revised land surface parameterization (SiB2) for atmospheric GCMs. Part I: Model formulation. *Journal of Climate*, *9*(4), 676–705. https://doi.org/10.1175/1520-0442(1996)009%3C0676:ARLSPF%3E2.0.CO;2

Seol, K., & Hong, S. Y. (2009). Relationship between the Tibetan snow in spring and the East Asian summer monsoon in 2003: A global and regional modeling study. *Journal of Climate*, *22*(8), 2095–2110. https://doi.org/10.1175/2008JCLI2496.1

Sun, Y., Fu, R., Dickinson, R., Joiner, J., Frankenberg, C., Gu, L., et al. (2015). Drought onset mechanisms revealed by satellite solar-induced chlorophyll fluorescence: Insights from two contrasting extreme events. *Journal of Geophysical Research: Biogeosciences*, *120*, 2427–2440. https://doi.org/10.1002/2015JG003150

Thapliyal, V. (2001). Long range forecast of summer monsoon rainfall over India: Evolution and development of a new power transfer model. *Proceedings Indian National Science Academy Part A*, *67*(3), 343–360.

Ting, M., & Wang, H. (1997). Summertime US precipitation variability and its relation to Pacific Sea surface temperature. *Journal of Climate*, *10*(8), 1853–1873. https://doi.org/10.1175/1520-0442(1997)010%3C1853:SUSPVA%3E2.0.CO;2

Trenberth, K. E., Branstator, W. G., & Arkin, P. A. (1988). Origins of the 1988 North American drought. *Science*, *242*(4886), 1640–1645. https://doi.org/10.1126/science.242.4886.1640

Von Storch, H., & Zwiers, F. Z. (1999). *Statistical analysis in climate research* (p. 484). New York: Cambridge University Press. https://doi.org/10.1017/CBO9780511612336

Walker, G. T., & Bliss, E. W. (1932). World weather V. *Memoirs of the Royal Meteorological Society*, *4*(1932), 53–84.

Wallace, J. M., & Gutzler, D. S. (1981). Teleconnections in the geopotential height field during the Northern Hemisphere winter. *Monthly Weather Review*, *109*(4), 784–812. https://doi.org/10.1175/1520-0493(1981)109%3C0784:TITGHF%3E2.0.CO;2

Wallace, J. M., Smith, C., & Bretherton, C. S. (1992). Singular value decomposition of wintertime sea surface temperatur and 500-mb height anomalies. *Journal of Climate*, *5*, 561–576.

Wang, S. W., Huang, W. R., Su, H. H., & Gillies, R. R. (2015). Role of the strengthened El Niño teleconnection in the May 2015 floods over the southern Great Plains. *Geophysical Research Letters*, *42*, 8140–8146. https://doi.org/10.1002/2015GL065211

Wu, G., Liu, Y., He, B., Bao, Q., Duan, A., & Jin, F. (2012). Thermal controls on the Asian summer monsoon. *Scientific Reports*, *2*(1), 404. https://doi.org/10.1038/srep00404

Wu, T.-W., & Qian, Z. (2003). The relation between the Tibetan winter snow and the Asian summer monsoon and rainfall: An observational investigation. *Journal of Climate*, *16*(12), 2038–2051. https://doi.org/10.1175/1520-0442(2003)016%3C2038:TRBTTW%3E2.0.CO;2

Xiao, Z., & Duan, A. (2016). Impacts of Tibetan Plateau snow cover on the interannual variability of the East Asian summer monsoon. *Journal of Climate*, *29*(23), 8495–8514. https://doi.org/10.1175/JCLI-D-16-0029.1

Xu, X., Zhao, T., Lu, C., Shi, X., Chen, B., & Ding, G. (2015). *Exploring the effect of Tibetan Plateau and its dynamical mechanisms* (In Chinese) (396 pp.). Beijing: China Meteorological Press.

Xue, Y., De Sales, F., Lau, W. K.-M., Boone, A., Kim, K.-M., Mechoso, C. R., et al. (2016). West African monsoon decadal variability and drought and surface-related forcings: Second West African Monsoon Modeling and Evaluation Project Experiment (WAMME II). *Climate Dynamics*, *47*(11), 3517–3545.

Xue, Y., De Sales, F., Vasic, R., Mechoso, C. R., Prince, S. D., & Arakawa, A. (2010). Global and temporal characteristics of seasonal climate/vegetation biophysical process (VBP) interactions. *Journal of Climate*, *23*(6), 1411–1433. https://doi.org/10.1175/2009JCLI3054.1

Xue, Y., Fennessy, M. J., & Sellers, P. J. (1996). Impact of vegetation properties on U.S. summer weather prediction. *Journal of Geophysical Research*, *101*(D3), 7419–7430. https://doi.org/10.1029/95JD02169

Xue, Y., Janjic, Z., Dudhia, J., Vasic, R., & De Sales, F. (2014). A review on regional dynamical downscaling in intraseasonal to seasonal simulation/prediction and major factors that affect downscaling ability. *Atmospheric Research*, *147-148*, 68–85. https://doi.org/10.1016/j.atmosres.2014.05.001

Xue, Y., Oaida, C. M., Diallo, I., Neelin, J. D., Li, S., De Sales, F., et al. (2016). Spring land temperature anomalies in northwestern US and the summer drought over Southern Plains and adjacent areas. *Environmental Research Letters*, *11*(4), 044018. https://doi.org/10.1088/1748-9326/11/4/044018

Xue, Y., Sellers, P. J., Kinter, J. L., & Shukla, J. (1991). A simplified biosphere model for global climate studies. *Journal of Climate*, *4*(3), 345–364. https://doi.org/10.1175/1520-0442(1991)004%3C0345:ASBMFG%3E2.0.CO;2

Xue, Y., Sun, S., Kahan, D., & Jiao, Y. (2003). The impact of parameterizations in snow physics and interface processes on the simulation of snow cover and runoff at several cold region sites. *Journal of Geophysical Research*, *108*(D22), 8859. https://doi.org/10.1029/2002JD003174

Xue, Y., Sun, S., Lau, J. M., Ji, J., Poccard, I., Kang, H. S., et al. (2005). Multiscale variability of the river runoff system in China and its link to precipitation and sea surface temperature. *Journal of Hydrometeorology*, *6*(4), 550–570. https://doi.org/10.1175/JHM439.1

Xue, Y., Vasic, R., Janjic, Z., Liu, Y. M., & Chu, P. C. (2012). The impact of spring subsurface soil temperature anomaly in the western U.S. on North American summer precipitation—A case study using regional climate model downscaling. *Journal of Geophysical Research*, *117*, D11103. https://doi.org/10.1029/2012JD017692

Xue, Y., Vasic, R., Janjic, Z., Mesinger, F., & Mitchell, K. E. (2007). Assessment of dynamic downscaling of the continental U.S. regional climate using the Eta/SSiB regional climate model. *Journal of Climate*, *20*(16), 4172–4193. https://doi.org/10.1175/JCLI4239.1

Xue, Y., Zeng, F. J., Mitchell, K., Janjic, Z., & Rogers, E. (2001). The impact of land surface processes on simulations of the U.S. hydrological cycle: A case study of the 1993 flood using the SSiB land surface model in the NCEP Eta regional model. *Monthly Weather Review*, *129*(12), 2833–2860. https://doi.org/10.1175/1520-0493(2001)129%3C2833:TIOLSP%3E2.0.CO;2

Xue, Y., Zeng, F. J., & Schlosser, C. A. (1996). SSiB and its sensitivity to soil properties—A case study using HAPEX-Mobilhy data. *Global and Planetary Change*, *13*(1–4), 183–194. https://doi.org/10.1016/0921-8181(95)00045-3

Yang, K., & Zhang, J. (2016). Spatiotemporal characteristics of soil temperature memory in China from observation. *Theoretical and Applied Climatology*, *126*(3–4), 739–749. https://doi.org/10.1007/s00704-015-1613-9

Yuan, F., Chen, W., Zhou, W., & W. (2012). Analysis of the role played by circulation in the persistent precipitation over South China in June 2010. *Advances in Atmospheric Sciences*, *29*(4), 769–781. https://doi.org/10.1007/s00376-012-2018-7

Zhang, L. X., & Zhou, T. J. (2015). Drought over East Asia: A review. *Journal of Climate*, *28*(8), 3375–3399. https://doi.org/10.1175/JCLI-D-14-00259.1

Zhao, P., Zhou, Z., & Liu, J. (2007). Variability of Tibetan spring snow and its associations with the hemispheric extratropical circulation and East Asian summer monsoon rainfall: An observational investigation. *Journal of Climate*, *20*(15), 3942–3955. https://doi.org/10.1175/JCLI4205.1